THE JOURNAL OF BIOLOGICAL CHEMISTRY
Vol. 271, No. 46, Issue of November 15, pp. 28977–28983, 1996
Printed in U.S.A.

The Regulatory Role for Magnesium in Glycolytic Flux of the Human Erythrocyte*

(Received for publication, March 21, 1996, and in revised form, August 7, 1996)

Maren R. Laughlin‡ and David Thompson

From the Department of Surgery, George Washington University Medical Center, Washington, D. C. 20037

^{31}P NMR was used to measure the intracellular free magnesium concentration ($[Mg^{2+}]_i$) in human erythrocytes while $[Mg^{2+}]_i$ was changed between 0.01 and 1.2 mM using the divalent cationophore A23187. ^{13}C NMR and [2-^{13}C]glucose were used to determine the kinetic effects of $[Mg^{2+}]_i$ by measuring the flux through several parts of the glucose pathway. Glucose utilization was strongly dependent on $[Mg^{2+}]_i$, with half-maximal flux occurring at 0.03 mM. The rate-limiting step was most likely at phosphofructokinase, which has a $K_{m(Mg^{2+})}$ of 0.025 mM in the purified enzyme. Phosphorylated glycolytic intermediate concentration was also strongly dependent on $[Mg^{2+}]_i$ and [MgATP], and glucose transport plus hexokinase may have been partially rate-determining at $[Mg^{2+}]_i$ below ~0.1 mM. The pentose phosphate shunt activity was too low to determine the dependence on $[Mg^{2+}]_i$. Phosphoglycerate kinase and 2,3-diphosphoglycerate mutase fluxes were also measured, but were not rate-limiting for glycolysis and showed no Mg^{2+} dependence. Human erythrocyte $[Mg^{2+}]_i$ varies between 0.2 mM (oxygenated) and 0.6 mM (deoxygenated), well above the measured $[Mg^{2+}]_{i(½)}$. It is unlikely, then, that $[Mg^{2+}]_i$ plays a regulatory role in normal erythrocyte glycolysis.

Many of the enzymes in the metabolic pathways that utilize glucose have a requirement for magnesium as demonstrated in kinetic studies of isolated enzymes (1–3). The K_m values for Mg^{2+} in the glycolytic enzymes of the human erythrocyte are between 1 and 2.3 mM for hexokinase (maximum activity at 37 °C = 11 μmol/h/ml of erythrocytes), 0.025 mM for phosphofructokinase (PFK)[1] (200 μmol/h/ml), 0.3 mM for phosphoglycerate kinase (PGK) (3000 μmol/h/ml), and 1 mM for pyruvate kinase (230 μmol/h/ml) (1, 3). $[Mg^{2+}]_i$ in oxygenated erythrocytes is 0.2 mM, which rises to 0.6 mM in the absence of oxygen due to the oxygen-dependent behavior of ATP binding to hemoglobin (4). Glucose utilization is concurrently increased by ~23–33% in the deoxygenated cell (5, 6). Since $[Mg^{2+}]_i$ is near the measured K_m for three of the potentially rate-limiting kinases and because both $[Mg^{2+}]_i$ and the glycolytic rate are modulated as oxygen tension changes, it stands to reason that $[Mg^{2+}]_i$ is important in erythrocyte glycolysis.

The divalent cationophore A23187 was used to change the concentration of intracellular Mg^{2+} in human erythrocytes, which are otherwise impermeable to magnesium. The distribution of Mg^{2+} across the cell membrane is then a function of membrane potential, V_m (Equation 1) (7).

$$[Mg^{2+}]_i = \exp(-2FV_m/RT)[Mg^{2+}]_e \quad \text{(Eq. 1)}$$

Intracellular Mg^{2+} was measured from the chemical shift of the ^{31}P NMR signals of the α- and β-phosphate groups of ATP (4). ^{13}C NMR was used to measure [2-^{13}C]glucose utilization and to estimate the flux through several of the enzyme systems in the glycolytic pathway at $[Mg^{2+}]_e$ between 0.01 and 1.00 mM: total glucose utilization, PFK flux, 2,3-DPG turnover, PGK flux, and pentose phosphate pathway flux (6).

EXPERIMENTAL PROCEDURES

Erythrocyte Preparation—7 ml of venous blood was taken from healthy volunteers who had given informed consent, under the guidelines of the George Washington University Medical Center IRB. After centrifugation, the resultant erythrocytes were washed twice in phosphate-buffered saline (pH 7.4) and once in experimental buffer (110 mM NaCl, 5 mM KCl, 40 mM HEPES, 15 mM Na_2HPO_4, 1 mM EGTA, and 5 mM adenine (pH 7.5)). Cells were diluted to 3% hematocrit in buffer containing 10 mM glucose, 6 μM A23187, and the appropriate Mg^{2+} concentration and incubated at 37 °C for 60 min in order to ensure equilibrium of Mg^{2+} across the cell membrane (7). Cells were then washed twice with the same buffer without glucose, resuspended at 50% hematocrit, and oxygenated by swirling in a 10-ml glass bulb on ice under hydrated oxygen. They were placed in a 10-mm NMR tube, and hydrated oxygen was passed over the cells during the NMR experiment.

NMR Experiment—All spectra were taken at 34 °C in a Bruker AC300 spectrometer equipped with a 10-mm proton low frequency probe that is tunable to either carbon or phosphorus. Two proton-decoupled ^{31}P NMR spectra were taken (10 min each, 60° pulse, 2-s relaxation delay, CPD decoupling). 10 mM [2-^{13}C]glucose was added, and 15 proton-decoupled ^{13}C NMR spectra were taken (10 min each, 60° pulse, 2-s relaxation delay, CPD decoupling, nuclear Overhauser effect development), followed by two final ^{31}P NMR spectra. Glucose, lactate, $Mg^{2+}{}_e$, pH, pO_2, and hematocrit were measured immediately before and after the experiment. The sample was stored at −50 °C until extracted with 6% perchloric acid.

Neutralized extracts were lyophilized and dissolved in 0.4 ml of ^2H_2O, and fully relaxed proton-decoupled ^{13}C NMR spectra were acquired (60° pulses, 10-s delays, CPD bilevel decoupling) for determination of the C-3/C-2 [^{13}C]lactate ratio used to calculate the pentose phosphate shunt activity.

Extracellular Magnesium Determination—A commercial electrode was used for determination of buffer free Mg^{2+} concentrations (NOVA Biomedical, Waltham, MA). The Mg^{2+}-sensitive divalent cation electrode in this instrument is also very sensitive to calcium concentration and ionic strength and is factory-calibrated for whole blood and plasma. We therefore constructed calibration curves for calcium-free solutions using 150 mM KCl in filtered, double-distilled water and stock solutions of $MgCl_2$ and $MgSO_4$. The calibration curves showed that the electrode mV readings deviated from the Nernst equation at the very low Mg^{2+} concentrations used, so buffer free magnesium values were estimated from a polynomial fit of electrode mV and $[Mg^{2+}]$.

Intracellular Mg^{2+} and MgATP Determination—$[Mg^{2+}]_i$ and [MgATP] were calculated from the chemical shift difference between α- and β-ATP, and total 2,3-DPG and ATP were measured in ^{31}P NMR

* The costs of publication of this article were defrayed in part by the payment of page charges. This article must therefore be hereby marked "*advertisement*" in accordance with 18 U.S.C. Section 1734 solely to indicate this fact.

‡ To whom correspondence should be addressed: Dept. of Surgery, George Washington University Medical Center, Ross Hall 550, 2300 Eye St., N. W., Washington, D. C. 20037. Tel.: 202-994-5774; Fax: 202-994-8974.

[1] The abbreviations used are: PFK, phosphofructokinase; PGK, phosphoglycerate kinase; $[Mg^{2+}]_i$, intracellular free magnesium concentration; $[Mg^{2+}]_e$, extracellular free magnesium concentration; 2,3-DPG, 2,3-diphosphoglycerate.

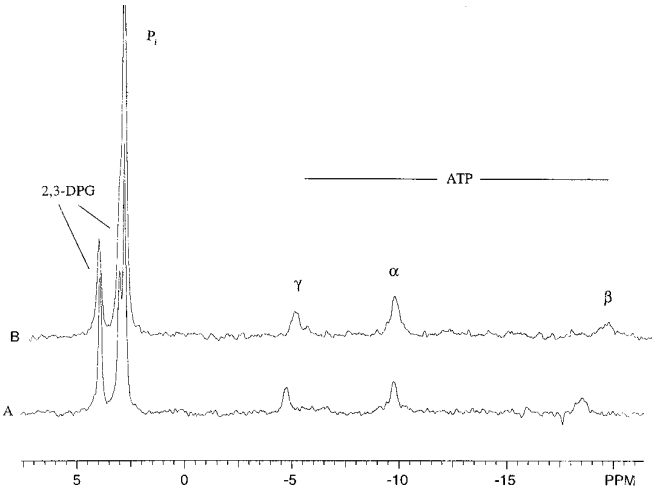

FIG. 1. **10-min ^{31}P NMR spectra of a 50% suspension of washed human erythrocytes taken at 121 MHz.** The *lower spectrum* shows cells incubated with 10 mM glucose and 1 mM EGTA and without added Mg^{2+}. Resonances from 2,3-DPG, P_i, and ATP are visible. The distance between the α- and β-ATP resonances is used to calculate $[Mg^{2+}]_i$, which is 0.19 mM. The *upper spectrum* shows the same cells after the addition of 6 μM A23187, where $[Mg^{2+}]_i$ has dropped to 0.02 mM.

spectra using the equations and dissociation constants found in Gupta *et al.* (4). A computer program written in Mathematica (Wolfram Research, Champaign, IL) was used to solve the four independent equations for each experiment. The limiting constants $\Delta ATP_{\alpha\beta}$ and $\Delta MgATP_{\alpha\beta}$ were corrected for pH_i (8), and pH_i was calculated from pH_e (9, 10).

Metabolite Concentrations—2,3-DPG was measured in trichloroacetic acid using a spectrophotometric method (Sigma) and corrected for the hematocrit, determined by a NOVA Stat 9 clinical analyzer. Total ATP was derived from the corrected 2,3-DPG/ATP ratio measured in ^{31}P NMR spectra. Hemoglobin concentration was assumed to be 7.02 mM (4).

NMR Data—The correction factors for saturation for both ^{31}P and ^{13}C NMR data were determined from spectra of solutions of commercially prepared metabolites in experimental buffer that contained no magnesium (Sigma). Spectra were acquired at 34 °C under the same conditions used for the NMR experiment (2-s delays), which were then repeated with a 15-s delay period. The solution for ^{31}P-labeled metabolites contained NaATP, 2,3-DPG (cyclohexylammonium salt), and Na_2HPO_4, and the ratios of the saturated to fully relaxed resonance intensities (normalized to 2,3-DPG) were used to correct the cell spectra. Saturation under our conditions required that the 2,3-DPG/ATP ratio be corrected by a factor of 1.6. The solution of ^{13}C-labeled metabolites contained [2-^{13}C]glucose, unlabeled lactate, and 2,3-DPG. Resonance areas were normalized to the β-[2-^{13}C]glucose peak, and correction ratios were 1.0 for [2-^{13}C]lactate and [2-^{13}C]DPG and 0.94 for α-[2-^{13}C]glucose.

Kinetic Data—Fluxes through several points of the glucose pathways were determined essentially as described by Schrader *et al.* (6). All fluxes are reported as μmol of glucose/min/g of hemoglobin to facilitate comparison between different parts of the pathway.

Glucose Utilization—α- and β-[2-^{13}C]glucose resonance areas were combined, and the results were normalized by setting peaks in the first ^{13}C NMR spectra (t = 0–10 min) equal to the total solution [glucose] measured at t = 0. The resultant concentrations were plotted against time and fit to a second-order polynomial. The early and late rates of glucose utilization were measured as the slope of this function at 30 and 120 min.

Pentose Phosphate Shunt and PFK Flux—The method of Schrader *et al.* (6) rests on the fact that the [2-^{13}C]glucose that passes through PFK yields 50% [2-^{13}C]lactate and 50% unlabeled lactate, whereas glucose loses its C-1 as CO_2 in the 6-phosphogluconate dehydrogenase reaction of the pentose phosphate pathway, yielding a family of [1-^{13}C]pentose 5-phosphates. These compounds then go on to form [1-^{13}C]Fru-6-P, [1,3-^{13}C]Fru-6-P, and unlabeled glyceraldehyde 3-phosphate. The Fru-6-P thus formed can return to the pentose phosphate shunt as Glc-6-P or continue through glycolysis. Therefore, the production of [3-^{13}C]lactate and [1-^{13}C]lactate is a measure of the pentose phosphate pathway. In Equations 2–4, PC is defined as the fraction of glucose uptake that

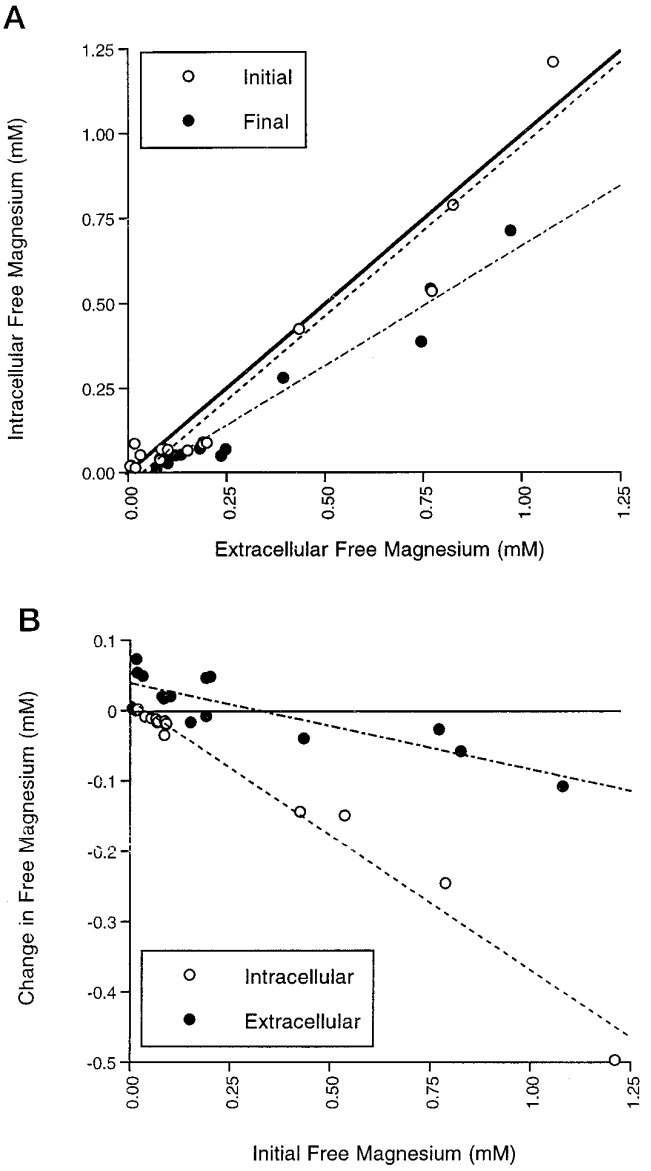

FIG. 2. *A*, the erythrocyte intracellular free Mg^{2+} concentration measured by ^{31}P NMR is plotted against the extracellular free Mg^{2+} concentration measured with a divalent cation-sensitive electrode at the beginning and end of a 150-min ^{13}C NMR glycolysis experiment. The lines are described by $[Mg^{2+}]_i = 0.996\ [Mg^{2+}]_e - 0.035$ ($r^2 = 0.940$) for data taken at the beginning and by $[Mg^{2+}]_i = 0.704\ [Mg^{2+}]_e - 0.036$ ($r^2 = 0.948$) at the end. *B*, the changes in intracellular and extracellular Mg^{2+} concentrations that occur during 150 min are plotted against the appropriate initial Mg^{2+} value. The intracellular Mg^{2+} concentration falls by the equation $\Delta[Mg^{2+}]_i = -0.383\ [Mg^{2+}]_{i(0)} + 0.014$ ($r^2 = 0.975$), whereas the extracellular Mg^{2+} concentration falls by the equation $\Delta[Mg^{2+}]_e = -0.123\ [Mg^{2+}]_{e(0)} + 0.039$ ($r^2 = 0.731$). The Mg^{2+} values at which $\Delta[Mg^{2+}] = 0$ are 0.037 mM (intracellular) and 0.32 mM (extracellular).

is converted to glyceraldehyde 3-phosphate (GAP).

$$3\ \text{Glc} \xrightarrow{\text{pentose pathway}} 3\ CO_2 + 2\text{Fru-6-P} + 1\ \text{GAP} \xrightarrow{\text{glycolysis}} 3\ CO_2 + 5\ \text{lactate} \quad \text{(Eq. 2)}$$

$$\frac{[3-{}^{13}\text{C}]\text{lactate}}{[2-{}^{13}\text{C}]\text{lactate}} - A = \frac{2\text{PC}}{1+2\text{PC}} \quad \text{(Eq. 3)}$$

$$\text{Flux into pentose pathway} = (3 \times \text{PC}) \times \text{glucose utilization} \quad \text{(Eq. 4)}$$

A is a correction factor of 0.03 to account for natural abundance ^{13}C at C-3. PFK flux can then be calculated from Equation 5.

$$\text{PFK} = \text{glucose utilization} \times (1 - \text{PC}) \quad \text{(Eq. 5)}$$

TABLE I
Metabolite concentrations

All values are means ± S.D. (n = 15).

Time	2,3-DPG	ATP	DPG/ATP	Hemoglobin	pH	Glucose	Lactate
min	*μmol/g hemoglobin*	*μmol/g hemoglobin*		*g/dl*		*mM*	*mM*
0	20.7 ± 2.8	5.4 ± 1.2	3.9 ± 0.6	16.9 ± 1.3	7.35 ± 0.04	13.1 ± 2.4	1.7 ± 0.5
150	19.7 ± 2.6	5.4 ± 1.4	3.8 ± 0.8	17.0 ± 1.3	7.15 ± 0.05	5.4 ± 2.2	13.7 ± 4.1

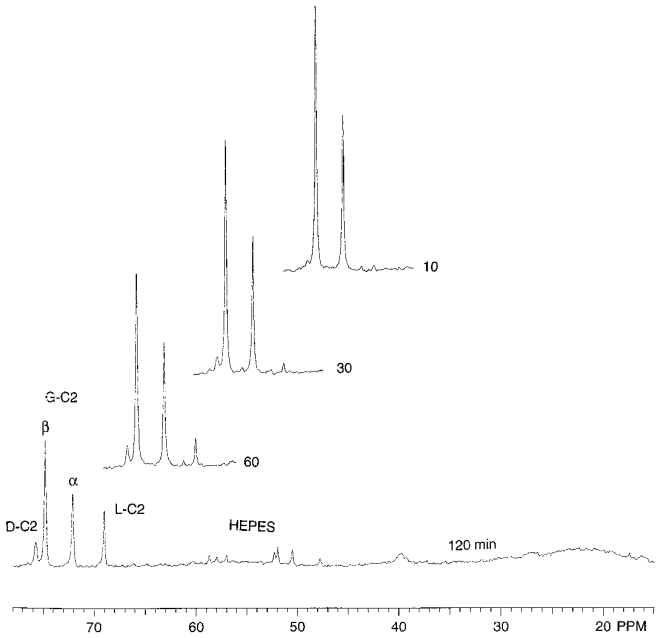

FIG. 3. **10-min ^{13}C NMR (75 MHz) spectra of a 50% suspension of washed human erythrocytes taken at 10, 30, 60, and 120 min of incubation with 10 mM [2-^{13}C]glucose, 1 mM EGTA, and 0.19 mM Mg^{2+}.** Shown are resonances from α- and β-[2-^{13}C]glucose (*G-C2*), which give rise in time to [2-^{13}C]lactate (*L-C2*) and 2,3-[2-^{13}C]DPG (*D-C2*). Also visible are the natural abundance ^{13}C carbons of HEPES in the incubation buffer (48–59 ppm), lipids (broad signal at 22 ppm), and hemoglobin (40 and 16 ppm).

2,3-DPG Bypass and Phosphoglycerate Kinase—In the erythrocyte, 2,3-DPG is produced from 1,3-DPG by 2,3-DPG mutase. This enzyme, along with 2,3-DPG phosphatase, constitutes a shunt past PGK, an ATP-producing reaction. Glycolysis produces 2 molecules of ATP/molecule of glucose, so the 2,3-DPG bypass allows glycolytic flux to proceed without net ATP production. The ^{13}C NMR experiment can be used to measure the ratio of the fluxes through 2,3-DPG mutase and PGK. The 2,3-[2-^{13}C]DPG time course is fit to a modification of Equation 6,

$$2,3\text{-}[2\text{-}^{13}\text{C}]\text{DPG}(t) = \frac{k_1 A_0}{k_2}(1 - \exp(-k_2 t)) \qquad \text{(Eq. 6)}$$

where A_0 is the concentration of the substrate (1,3-DPG), and k_1 and k_2 are the rate constants for 2,3-DPG mutase and phosphatase, respectively (6). This equation did not produce a good fit to the NMR data. A better fit was made to Equation 7, where the rate of label flowing into the 2,3-DPG pool was assumed to be linearly changing, rather than a constant. Presumably, this is due to the changing pH that occurs throughout the experiment and affects the PFK flux. The parameters are k_1A_0, k_2A_0, and k_3.

$$2,3\text{-}[2\text{-}^{13}\text{C}]\text{DPG} = \frac{(k_1 t + k_2)A_0}{k_3}(1 - \exp(-k_3 t)) \qquad \text{(Eq. 7)}$$

The initial rate is given by k_2A_0. The sum of [2-^{13}C]lactate and 2,3-[2-^{13}C]DPG was fit to a second-order polynomial, and the difference in initial rates yields the fractional PGK flux ([2-^{13}C]lactate labeling), which can be multiplied by total triose flux ((2 − PC) × glucose utilization) to yield net ATP production.

Control Strength of $[Mg^{2+}]_i$—The fluxes through different points of the glucose pathway were plotted *versus* $[Mg^{2+}]_i$ and fit to both the Michaelis-Menten equation (Equation 8) and to two simple straight lines, which would be similar to estimating a fit "by eye." The Michaelis-Menten formalism is generally applicable only to initial rates measured for a single isolated enzyme with one substrate, but the general form is similar to that for a more complicated enzyme series that contains a single rate-limiting step, with a single limiting substrate. It cannot be expected to fit data gleaned from a whole cell. The use of either Equation 8 or two simple straight lines yields a similar $[Mg^{2+}]_{i(½\text{-MM})}$ or $[Mg^{2+}]_i$ at half-maximal velocity.

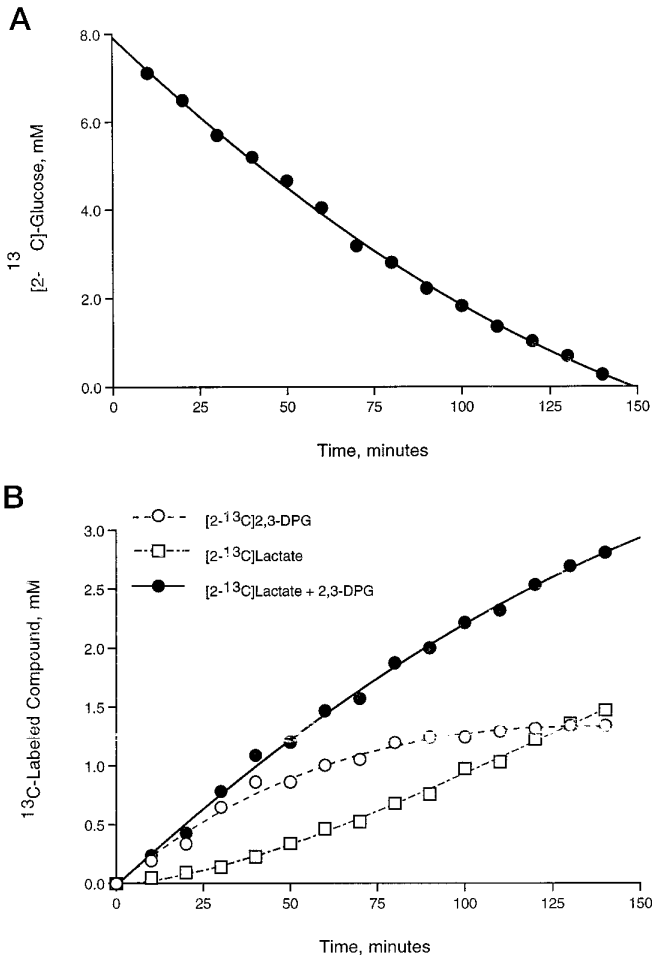

FIG. 4. **The ^{13}C NMR signals were calibrated and fit to appropriate functions.** *A*, [2-^{13}C]glucose, fit to a second-order polynomial, is plotted. Rates were calculated as the tangent to this function at 30 and 120 min. *B*, [2-^{13}C]lactate and 2,3-[2-^{13}C]DPG are plotted. 2,3-DPG was fit to Equation 7, and the sum of 2,3-DPG and lactate was fit to a second-order polynomial. Lactate falls along the difference of these two fits.

$$\text{Flux} = \frac{V_{max} \times [Mg^{2+}]_i}{[Mg^{2+}]_{i(½\text{-MM})} + [Mg^{2+}]_i} \qquad \text{(Eq. 8)}$$

Fluxes were also plotted against calculated [MgATP] and analyzed by simple linear regression. $[Mg^{2+}]_{i(½)}$ was found from the point on the line at half-maximal flux.

RESULTS

Free Magnesium—Fig. 1 shows 10-min ^{31}P NMR spectra of a 50% suspension of washed human erythrocytes taken before

and after the addition of A23187 in the presence of 1 mM EGTA and without added Mg^{2+}. $[Mg^{2+}]_i$ was determined from $\Delta ATP_{\alpha\beta}$ in ^{31}P NMR spectra by the method of Gupta *et al.* (4), which accounts for the selective oxygen-dependent binding of 2,3-DPG and ATP to hemoglobin. Fig. 2*A* shows $[Mg^{2+}]_e$ estimated with a divalent cation electrode and $[Mg^{2+}]_i$ measured at the beginning and end of the 150-min glycolysis period. Although the relationship between $[Mg^{2+}]_e$ and $[Mg^{2+}]_i$ is originally close to unity, it changes during the course of the experiment. Fig. 2*B* shows the change during the experiment in both intra- and extracellular $[Mg^{2+}]$ plotted against the appropriate initial concentration. While $[Mg^{2+}]_i$ decreases in every case, $[Mg^{2+}]_e$ appears to be buffered by the erythrocyte and changes in such a way as to approach 0.32 mM. For both intra- and extracellular magnesium ions, this delta is a direct function of the original concentration.

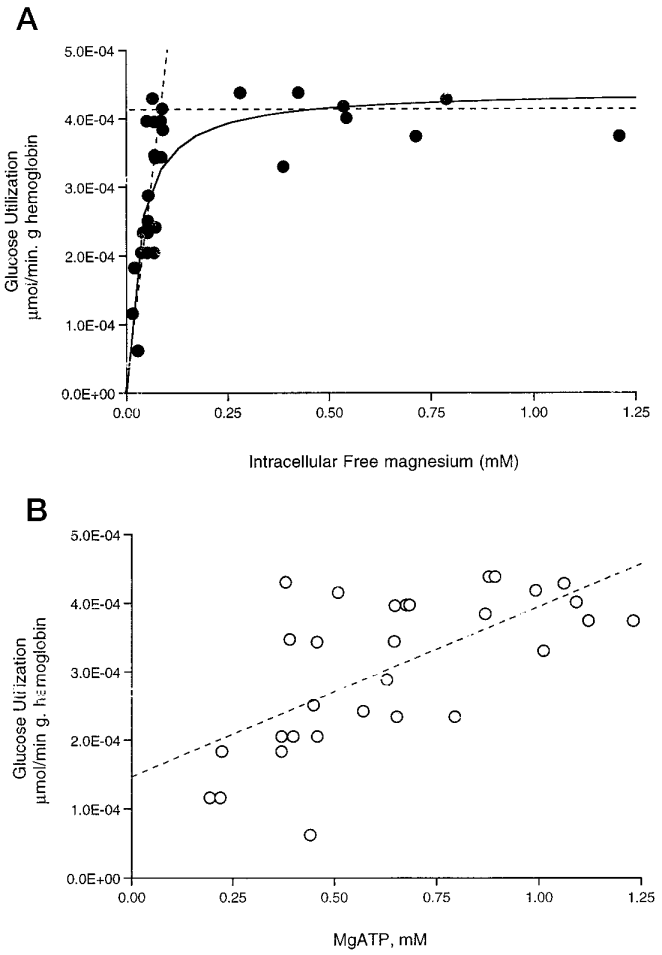

FIG. 5. *A*, the glucose utilization rates measured at 30 and 120 min as described for Fig. 4*A* are plotted against $[Mg^{2+}]_i$ measured at the beginning and end of the experiment. The data were fit both to the Michaelis-Menten equation (*solid curve*) and to two simple straight lines (*dashed lines*). Results are shown in Table II. *B*, shown is glucose utilization as a function of calculated [MgATP]. A simple linear regression yielded the *dashed line*.

Table I shows the average pH and ATP, 2,3-DPG, hemoglobin, glucose, and lactate concentrations at 0 and 150 min for all 15 experiments. Although there was variation between samples, there were few changes in high energy phosphates during the experiment. The glycolytic rate is substantially depressed by acidic pH (as much as 250% rate change/pH unit (9, 11)), yet the change in pH in our experiments due to lactate production correlated positively with the rate of glycolysis ($r^2 = 0.81$). Therefore, there was a tendency toward lower pH and probably slightly lower glycolytic fluxes measured toward the end of the experiments with the highest magnesium levels.

Glycolysis—Fig. 3 shows ^{13}C NMR spectra taken at 10, 30, 60, and 120 min after the addition of [2-^{13}C]glucose, and Fig. 4 (*A* and *B*) shows the time courses and characteristic fits of the [2-^{13}C]glucose, [2-^{13}C]lactate, and 2,3-[2-^{13}C]DPG resonance areas.

Fig. 5*A* shows the [2-^{13}C]glucose utilization rates measured at 30 and 120 min of each experiment plotted against the appropriate $[Mg^{2+}]_i$. These data were fit both to a Michaelis-Menten equation and to two straight lines. The second, linear fit is statistically better in most cases and is likely to be no less appropriate than the Michaelis-Menton equation, given the complex intact cell system being studied. Table II shows the V_{max} and $[Mg^{2+}]_{i(½\text{-MM})}$ for the Michaelis-Menten fit and the $[Mg^{2+}]_{i(½)}$ for the linear fit.

Because many enzymes in the glycolytic pathway are dependent on both MgATP and Mg^{2+}, [MgATP] was calculated for each experiment from measured Mg^{2+}, pH, and total ATP and 2,3-DPG using the equations from Gupta *et al.* (4) and LaNoue and co-workers (8). As can be seen in Fig. 6, when [MgATP], calculated assuming a constant total ATP concentration of 2.08 mM (4), is plotted against $[Mg^{2+}]$, it has a shape that is similar to the dependence of glucose utilization on $[Mg^{2+}]_i$. The glucose utilization rates are replotted against [MgATP] in Fig. 5*B* and show a correlation as expected.

TABLE II

Kinetic parameters for fluxes through various pathways in the erythrocyte

Data are from Figs. 5 and 8–10. V_{max} and $[Mg^{2+}]_{i(½\text{-MM})}$ are from Michaelis-Menten fits of flux *versus* $[Mg^{2+}]_i$. V_{max} is always expressed as µmol of glucose equivalents/min/g of hemoglobin for easy comparison of fluxes through different enzymes. $[Mg^{2+}]_{i(½)}$ is Mg^{2+} at half-maximal velocity found in line fits of flux *versus* $[Mg^{2+}]_i$. The slope is taken from linear regression of flux *versus* calculated [MgATP] and is accompanied by the correlation coefficient.

	V_{max}	$[Mg^{2+}]_{i(½\text{-MM})}$, Michaelis-Menten fit	$[Mg^{2+}]_{(½)}$ Linear fit	Slope
	µmol glucose/min/g hemoglobin	*mM*	*mM*	*µmol/min/g hemoglobin/mM MgATP*
[2-^{13}C]Glucose utilization	4.40×10^{-4}	0.030	0.035	2.48×10^{-4} ($r^2 = 0.430$)
PFK flux	4.38×10^{-4}	0.030	0.036	2.48×10^{-4} ($r^2 = 0.429$)
2,3-DPG mutase flux	3.52×10^{-4}	0.023	0.027	1.55×10^{-4} ($r^2 = 0.330$)
PGK flux	0.8×10^{-4}			0.70×10^{-4} ($r^2 = 0.170$)
Phosphomonoester concentration				0.21 ($r^2 = 0.673$)

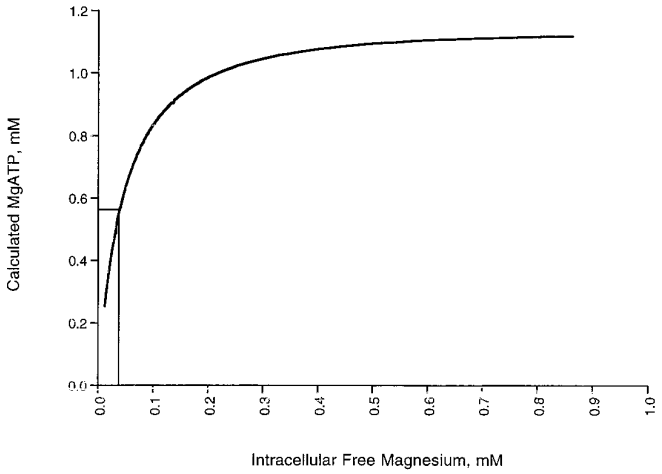

FIG. 6. **Calculated [MgATP] as a function of [Mg^{2+}].** [MgATP] was calculated from [Mg^{2+}] assuming a constant total ATP concentration of 2.09 mM (4). [Mg^{2+}] at half-maximal [MgATP] is 0.04 mM, similar to fits of glucose utilization (see Fig. 5*A*).

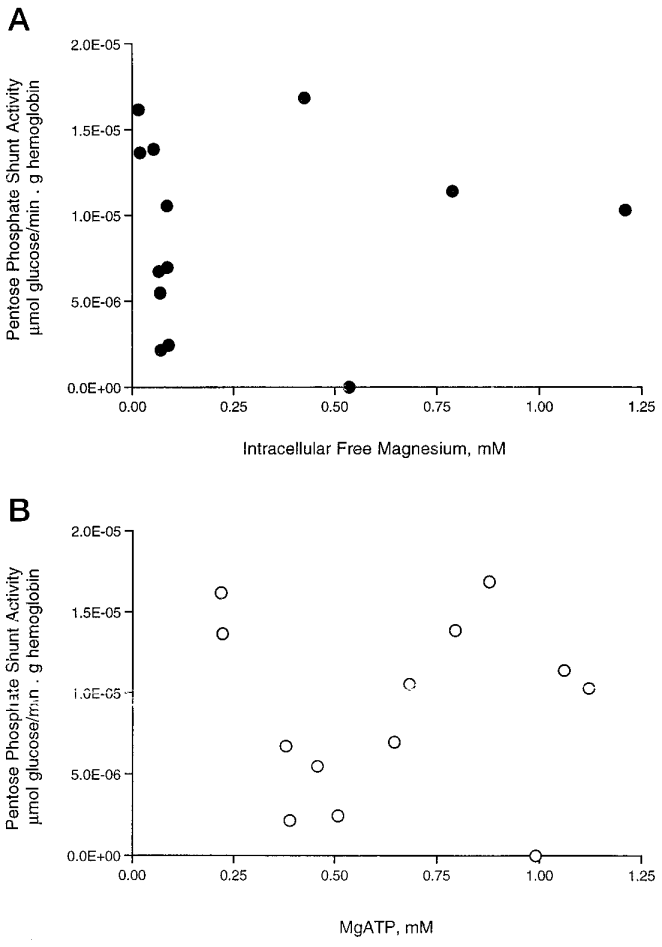

FIG. 7. **Pentose phosphate shunt activity calculated from the ratio of C-3 to C-2 of [^{13}C]lactate and shown as a function of [Mg^{2+}]$_i$ (*A*) and calculated [MgATP] (*B*).**

Pentose Phosphate Shunt—The pentose phosphate shunt activity can be measured from the flux of label from [2-^{13}C]glucose into [1-^{13}C]triose and [3-^{13}C]triose. However, there was no [1-^{13}C]lactate, [3-^{13}C]lactate, or 2,3-DPG visible in any of the cell suspension spectra. In spectra of perchloric acid extracts, a small amount of [3-^{13}C]lactate was observable, but [1-^{13}C]lactate was never observed. The average pentose phosphate flux calculated for each experiment in extracts is plotted against the

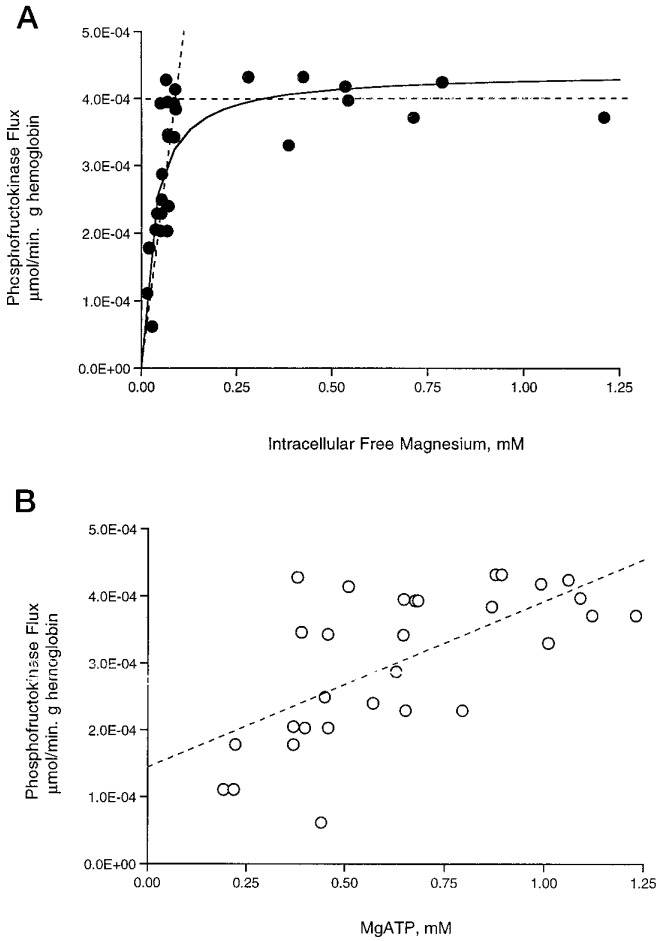

FIG. 8. **Phosphofructokinase flux shown *versus* [Mg^{2+}]$_i$ (*A*) and calculated [MgATP] (*B*).** The *solid curve* represents the fit to the Michaelis-Menten equation, and the *dashed lines* are simple linear fits. Results are shown in Table II.

average [Mg^{2+}]$_i$ and [MgATP] in Fig. 7 (*A* and *B*).

PFK—PFK is plotted against [Mg^{2+}]$_i$ and [MgATP] in Fig. 8. PFK has an apparent [Mg^{2+}]$_{i(½)}$ similar to glucose utilization (Table II).

PGK, 2,3-DPG Shunt, and ATP Production—The initial rates for 2,3-[2-^{13}C]DPG and [2-^{13}C]lactate appearance in ^{13}C NMR spectra (Figs. 3 and 4) yield the fluxes through 2,3-DPG mutase and PGK. Fig. 9 shows these rates plotted as a function of PFK flux. Flux through both enzymes appears to be a constant fraction of PFK flux, and therefore, the ratio of the two exhibits no clear unique dependence on [Mg^{2+}]$_i$ or [MgATP]. On average, 75.3% of all carbons pass through the 2,3-DPG shunt, and 24.3% flow through PGK.

Phosphomonoesters: PFK Versus Hexokinase—The phosphomonoester metabolites were very difficult to quantitate in the ^{31}P NMR spectrum (4–6 ppm) due to the many small broad peaks. It was not possible to measure changes in individual phosphorylated glycolytic intermediates, but it was possible to report the area under the entire phosphomonoester region. Fig. 10 shows these estimates. The metabolites in this region are reduced to very low levels during 150 min of glycolysis at the low magnesium levels and are elevated well above the control values at the highest [Mg^{2+}]$_i$. Total phosphomonoester correlated well with MgATP.

DISCUSSION

Erythrocyte glycolysis depends on [Mg^{2+}]$_i$, with an overall [Mg^{2+}]$_{i(½)}$ of ~0.03 mM, which is an order of magnitude below physiologically important levels. In the normal oxygen delivery

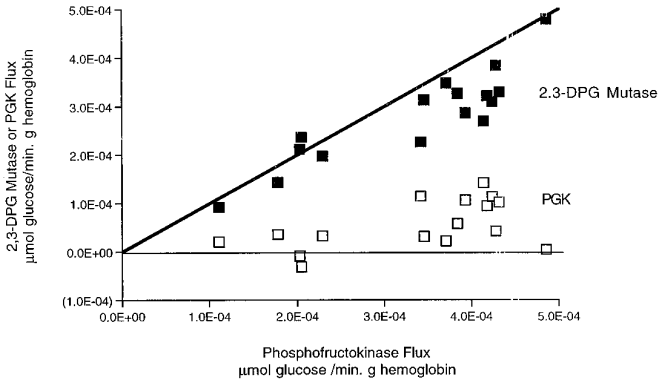

FIG. 9. **Fluxes through 2,3-DPG mutase (*closed squares*) and PGK (*open squares*) calculated from ^{13}C NMR data as shown in Fig. 4*B* and plotted against PFK flux.** The data are described by the following lines: 2,3-DPG mutase = 0.7531 PFK + 2.88 × 10^{-5} (r^2 = 0.795) and PGK = 0.243 × PFK − 2.64 × 10^{-5} (r^2 = 0.284).

cycle, $[Mg^{2+}]_i$ varies between 0.2 mM (oxygenated) and 0.6 mM (deoxygenated) (4), but at constant oxygen tension, appears to be well buffered. Erythrocytes contain ~3.5 mmol of total magnesium/kg of water and three to four distinct pools of buffering molecules: 100 µM buffer with $K_m \approx 0.03$ µM, 2 mM buffer with $K_m \approx 25$–50 µM, and ~20–30 mM buffer with $K_m \approx 1$–4 mM (7). Under certain pathological conditions, human erythrocyte $[Mg^{2+}]_i$ can decrease, but falls to only 0.13 ± 0.02 mM in renal magnesium loss (12) or to 0.16 mM after 3 weeks of magnesium deficiency (13).

Calculated [MgATP] correlates well with PFK flux (Fig. 8) and NMR-visible phosphomonoesters (Fig. 10). MgATP concentration is ~0.48 mM at $[Mg^{2+}]_{i(½)}$ = 0.03 mM in oxygenated cells. In the normal course of oxygenation/deoxygenation, it varies between 1.0 and 0.8 mM (4), which may be in the regulatory range.

Integration of the phosphomonoester region indicates that the phosphorylated intermediates including such compounds as Glc-6-P (4.7 ppm) and DHAP (4.37 ppm) increase during the incubation with glucose at high $[Mg^{2+}]_i$ and decrease at low $[Mg^{2+}]_i$. The crossover point is ~0.1 mM Mg^{2+} or ~0.5 mM MgATP. Even though glucose utilization is very slow at low $[Mg^{2+}]_i$, the concentration of phosphorylated glycolytic intermediates falls, indicating that transport and/or phosphorylation of glucose (these steps cannot be distinguished in the present experiment) is lagging behind other potentially rate-limiting steps. At higher $[Mg^{2+}]_i$, the rate-limiting step must be later in the glycolytic pathway since phosphorylated intermediate pools build up. This implies that the combination of transport and phosphorylation of glucose is at least partially rate-limiting for glycolysis at low $[Mg^{2+}]_i$. The $K_{a(Mg^{2+})}$ for purified hexokinase from human erythrocytes is between 1.0 and 2.3 mM, with a Mg^{2+} dependence observed up to 4 mM, and the $K_{m(MgATP)}$ is between 1 and 2 mM (1, 2). Since at even the highest $[Mg^{2+}]_i$ studied the change in phosphomonoesters had not reached a maximum, our results in the intact cell are consistent with this rather high $K_{a(Mg^{2+})}$ for hexokinase (Fig. 10). This activation of the early steps in glycolysis may be important for increasing glycolytic intermediates in deoxygenated cells, which have much higher $[Mg^{2+}]_i$ and higher glycolytic rates.

The ^{13}C NMR experiment does not clearly indicate which step in the glycolytic pathway is rate-limiting. It may in fact change throughout the experiment; lactate accumulation changes the intracellular NADH/NAD^+ ratio and inhibits glyceraldehyde-3-phosphate dehydrogenase (10). On the other hand, decreases in pH have the greatest effect on PFK (11). The present experiments do demonstrate a distinct Mg^{2+} dependence of glycolysis, and PFK has a clear dependence on Mg^{2+} and MgATP, while glyceraldehyde-3-phosphate dehydrogenase does not. The $K_{m(Mg^{2+})}$ for purified human erythrocyte PFK has been reported to be 0.025 mM (1). In an analysis of the kinetics of PFK from rat erythrocytes, it appeared that Mg^{2+} in itself did not directly activate the enzyme (3). It instead served three distinct roles: as part of the substrate MgATP ($K_{m(MgATP)}$ = 0.07 mM), to release inhibition by uncomplexed ATP ($K_{i(ATP)}$ = 0.01 mM), and to inhibit PFK ($K_{i(Mg^{2+})}$ = 0.44 mM). In the present study, there was no apparent decline in PFK flux at $[Mg^{2+}]_i$ near or above the reported K_i, and the MgATP and ATP concentrations at half-maximal velocity were on the order of 0.4 and 0.6 mM, respectively, well above the reported activation and inhibition coefficients. Our results do not support this second model of PFK regulation. However, because of the similarity of our measured $[Mg^{2+}]_{i(½)}$ to the reported K_m for the isolated human enzyme, PFK does appear to be the primary rate-determining enzyme under our experimental conditions (1).

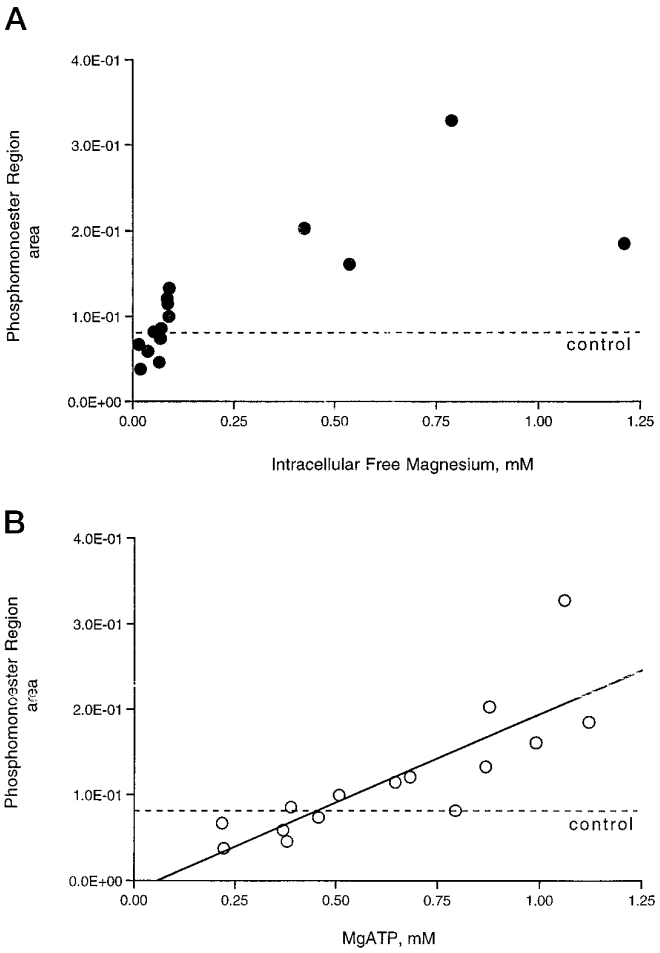

FIG. 10. **Total area of signals found in the phosphomonoester region (sugar phosphates and other phosphorylated glycolytic intermediates) in the final ^{31}P NMR spectra plotted against $[Mg^{2+}]_i$ (*A*) and calculated [MgATP] (*B*).** The relationship with $[Mg^{2+}]_i$ is biphasic, but phosphomonoesters are linear with [MgATP] (phosphomonoester = 0.21 [MgATP] − 0.01 (r^2 = 0.673)). Signals increase during the experiment at high $[Mg^{2+}]_i$ and decrease when $[Mg^{2+}]_i$ is low. Normal [MgATP] in the oxygenated erythrocyte is ~1 mM.

The pentose phosphate pathway and PGK flux were too low to solidly define their Mg^{2+} dependence in the present experiments. It is interesting that unlike other cells that do not have the 2,3-DPG shunt, low activity of PGK does not limit glycolytic flux in the erythrocyte. Purified PGK has a strong dependence

on Mg^{2+}, with a reported $K_{m(Mg^{2+})}$ of 0.3 mM and $K_{m(MgATP)}$ = 0.44 mM (1). Our data show no rate dependence around these points, indicating that PGK flux is being limited by something else. Since PGK is the point at which net ATP production is regulated, perhaps its flux is limited by low ATP utilization in these experiments. PGK flux is more or less linear with PFK flux (Fig. 9), which implies that the concentration of the substrate 1,3-diphosphoglycerate is important.

In many studies, including one done with ^{13}C NMR, the time-averaged pentose phosphate shunt activity was significant, ~17% of total glucose utilization in oxygenated human erythrocytes (5, 6, 14), whereas in the present study, it was at most 4%. This may be due to differences in the experimental design. The previous experiments were carried out for very long periods of time, and it appears from the time courses of [2-^{13}C]lactate and [3-^{13}C]lactate that the pentose phosphate shunt activity was increased at the later times, when 2,3-DPG was falling and P_i was probably rising. It was important to keep 2,3-DPG, total ATP, and P_i constant in these experiments because all three regulate glycolysis. 2,3-DPG inhibits PFK, hexokinase, PGK, and pyruvate kinase. PGK and pyruvate kinase may be inhibited by ~80% at the normal 2,3-DPG concentrations (1). P_i inhibits PFK and strongly stimulates hexokinase (11). It is possible that as high energy phosphates fall and P_i increases, pentose phosphate shunt activity is increased.

A second explanation for the low pentose phosphate shunt activity is the low rate of Ca^{2+} pumping that takes place in the presence of 1 mM EGTA. When A23187 and even the minute calcium concentrations found in deionized water are present simultaneously, erythrocyte heat and lactate production are both increased, and ATP falls precipitously due to a very active ATP-dependent Ca^{2+}-H^+ exchanger in the membrane (15–17). Normal erythrocyte intracellular Ca^{2+} is maintained at vanishingly low levels by this Ca^{2+} pump and an impermeable cell membrane in the face of ~1.2 mM ion in the plasma. The basal level of the Ca^{2+}-ATPases most likely causes some turnover of nucleotides and associated pentose phosphate pathway activity, which would be absent in the present experiments (14).

The slope of the intracellular *versus* extracellular free magnesium concentration is a measure of the square of the Donnan potential (r), which is a function of membrane potential, and is highly dependent on pH, ion concentrations, and cell volume (7). The Donnan potential has apparently changed during the experiment from 0.90 to 0.76. If true, this would largely explain the tight correlation between the change in $[Mg^{2+}]_i$ and its initial concentration (r^2 = 0.983). However, $[Mg^{2+}]_e$ also changes, but in such a way as to approach the concentration 0.32 mM. This implies a large extracellular buffer for magnesium with a K_D in the range of its normal plasma concentration (0.5 mM). The existence of such a buffer has been noted in the literature (18) and may consist of membrane-bound phospholipids. We hoped to fill all magnesium sites in the cells by a long preincubation at the experimental magnesium ion and ionophore concentrations. The changes in $[Mg^{2+}]_e$ may therefore indicate a shift in the binding site concentration or dissociation constant. Clearly, it cannot be assumed that either $[Mg^{2+}]_e$ or $[Mg^{2+}]_i$ is constant when experiments with A23187 are conducted for long periods of time at high hematocrits.

The ionophore seems to increase glycolysis; in our studies, it went up ~100% from 2.1×10^{-4} in controls (data not shown) to 4×10^{-4} mmol/min/g of hemoglobin. This is similar to the results of Engstrom *et al.* (15, 16), who found an increase in glycolysis from 6.7×10^{-5} to 1.3×10^{-4} mmol/min/g of hemoglobin in the presence of A23187 and 3 mM Mg^{2+}. It was also noted that the rates of glucose and [2-^{13}C]glucose utilization are always greater than production of total lactate or labeled trioses (see Fig. 3 and Table I). This is not a new finding (6, 10). Since there is no apparent large increase in [2-^{13}C]pyruvate or other labeled intermediates, it probably indicates slow lactate transport across the membrane or binding of lactate to cellular components accompanied by a decrease in NMR visibility of the bound fraction.

In summary, $[Mg^{2+}]_{i(1/2)}$ has been determined for glycolysis in the human erythrocyte and found to be 0.03 mM. The rate-limiting site is most likely to be PFK. Pentose phosphate shunt activity was too low to explore the magnesium dependence under these experimental conditions. 2,3-DPG mutase and PGK flux were not rate-limiting and therefore showed no Mg^{2+} dependence. Glucose transport and phosphorylation, as determined by concentration of and changes in total phosphomonoester compounds, have a strong dependence on $[Mg^{2+}]_i$ and [MgATP]. These results indicate that there is a strong regulatory role for $[Mg^{2+}]_i$ in the glycolytic pathways of the erythrocyte, but that $[Mg^{2+}]_{i(1/2)}$ is far lower than the normal range of $[Mg^{2+}]_i$ in the cell.

Acknowledgments—We thank Michael Salem, Anita Phillip, and Steven Malekzaleh for contributions to this work.

REFERENCES

1. Ponce, J., Roth, S., and Harkness, D. R. (1971) *Biochim. Biophys. Acta* **250,** 63–74
2. Gerber, G., Preissler, H., Heinrich, R., and Rapoport, S. M. (1974) *Eur. J. Biochem.* **45,** 39–52
3. Otto, M., Heinrich, R., Kuhn, B., and Jacobasch, G. (1974) *Eur. J. Biochem.* **49,** 169–178
4. Gupta, R. K., Benovic, J. L., and Rose, Z. B. (1978) *J. Biol. Chem.* **253,** 6172–6176
5. Murphy, J. R. (1960) *J. Lab. Clin. Med.* **55,** 286–302
6. Schrader, M. C., Eskey, C. J., Simplaceanu, V., and Ho, C. (1993) *Biochim. Biophys. Acta* **1182,** 162–178
7. Flatman, P., and Lew, V. L. (1977) *Nature* **267,** 360–362
8. Mosher, T. J., Williams, G. D., Doumen, C., LaNoue, K. F., and Smith, M. B. (1992) *Magn. Reson. Med.* **24,** 163–169
9. Grimes, A. J. (1960) *Anaerobic Glycolysis in Human Red Cell Metabolism*, Blackwell Scientific Publications, New York
10. Tilton, W. M., Seaman, C., Carriero, D., and Piomelli, S. (1991) *J. Lab. Clin. Med.* **118,** 146–152
11. Minakami, S., and Yoshikawa, H. (1966) *J. Biochem. (Tokyo)* **59,** 145–150
12. Geven, W. B., Vogels-Mentink, W. B., Willems, J. L., Os, C. H. v., Hilbers, C. W. Joordens, J. J. M., Rijksen, G., and Monens, L. A. H. (1991) *Clin. Chem.* **37,** 206–208
13. Rude, R. K., Stephen, A., and Nadler, J. (1991) *Magnesium Trace Elem.* **92,** 117–121
14. Palsson, B. O., Narang, A., and Joshi, A. (1989) *The Red Cell: Seventh Ann Arbor Conference*, pp. 133–154, Alan R. Liss, Inc., New York
15. Engstrom, I., Waldenstrom, A., Nilsson-Ehle, P., and Ronquist, G. (1993) *Clin. Chim. Acta* **219,** 113–122
16. Ferreira, H. G., and Lew, V. L. (1976) *Nature* **259,** 47–49
17. Engstrom, I., Waldenstrom, A., and Ronquist, G. (1993) *Scand. J. Clin. Lab. Invest.* **5,** 239–246
18. Tongyhai, S., Rayssiguier, Y., Motta, C., Gueux, E., Maurois, P., and Heaton, F. W. (1989) *Am. J. Physiol.* **257,** C270–C276